JOURNAL OF APPLIED ELECTROCHEMISTRY **29** (1999) 27–34

# Turbulent free convection in large electrochemical cells with a binary electrolyte

F. GURNIKI, F. H. BARK

*FaxénLaboratoriet, Royal Institute of Technology, Stockholm, S-10044 Sweden*
*E-mail: anakar@mech.kth.se*

S. ZAHRAI

*ABB, Corporate Research, S-72178 Västerås, Sweden*

Received 24 March 1997; accepted in revised form 30 April 1998

A mathematical model proposed by Bark and Alavyoon for modelling laminar natural convection in electrochemical cells, with binary electrolytes, is extended to simulation of two-dimensional turbulent flows. The turbulence was modelled by a standard $k$–$\epsilon$ model. The constants used in the model are the same as those used by Henkes and Hoogendoorn. Steady state calculations were carried out in a square, differentially heated enclosure for $Gr = 7 \times 10^{10}$ and $Pr = 0.71$. The turbulence model used could not predict the transition effect on the Nusselt number along the hot wall. Transient calculations performed in an enclosure with an aspect ratio of 35, for $Gr = 6.4 \times 10^{11}$ and $Sc = 2763$, revealed large scale fluctuations in the boundary layers near the vertical walls. The model was able to predict qualitatively the velocity field for transitional flow for air induced by buoyancy at $Gr_h = 8100$ and $Gr_h = 22\,500$. The correlation between the Sherwood and Rayleigh numbers was studied by modelling the mass transfer at the electrodes using a Butler–Volmer law. The computed Sherwood number was found to be approximately proportional to the Rayleigh number to the power of 0.2 in the range of $Ra_h$ between $5 \times 10^8$ and $10^{10}$, and with an order of magnitude of $10^5$.

Keywords: *natural convection*, *turbulence k–ϵ model*, *current density*, *Butler–Volmer law*, *electrical potential*

**List of symbols**

| | |
|---|---|
| $c$ | concentration (mol m$^{-3}$) |
| $\mathscr{C}$ | a reference value for the metallic ionic species $\min\left[\frac{hi_0}{FD_1} \times \sinh\left[\frac{F}{RT}(V_+ - V_-)\right], c_0\right]$ (mol m$^{-3}$) |
| $C_f$ | dimensionless wall-shear stress defined by $H(\partial v/\partial x)_w/\sqrt{g\beta\Delta TH}$ |
| $C_1, C_2$ | coefficients in $\epsilon$ equation |
| $C_\mu$ | coefficient in $v_T$ equation |
| $D$ | salt diffusivity defined by $\frac{D_1D_2(z_1-z_2)}{D_1z_1-D_2z_2}$ (m$^2$ s$^{-1}$) |
| $E$ | electrode potential (V) |
| $F$ | Faraday constant (96 485 C mol$^{-1}$) |
| $g$ | acceleration due to gravity (9.81 m s$^{-2}$) |
| $Gr$ | Grashof number $Ra/Sc$ |
| $Gr_h$ | Grashof number $Ra_h/Sc$ |
| $H$ | half-height of the cell (m) |
| $h$ | half-width of the cell (m) |
| $i_0$ | exchange current density (A m$^{-2}$) |
| $j_L$ | limiting current density due to mass transport (A m$^{-2}$) |
| $\vec{i}$ | current density vector |
| $k$ | turbulent kinetic energy (m$^2$ s$^{-2}$) |
| $k_m$ | rate constant for mass transport $\frac{j_L}{z_1FC_0}$ (m s$^{-1}$) |
| $\|\|\vec{N}_i\|\|$ | mass flux of species $i$ (mol m$^{-2}$ s) |
| $Nu$ | Nusselt number defined by $-(H/\Delta T)\,[\partial T/\partial x]_w$ |
| $\vec{n}$ | normal direction to the wall |
| $p$ | pressure (N m$^{-2}$) |
| $P$ | coefficient appearing in equation for electric potential $\frac{z_1(D_1-D_2)}{D_1z_1-D_2z_2}$ |
| $R$ | gas constant (8.31 J mol$^{-1}$ K$^{-1}$) |
| $Ra$ | Rayleigh number $\rho_0\mathscr{C}g(2H)^3(\alpha_1+\alpha_2)/2\mu D$ |
| $Ra_h$ | Rayleigh number $\rho_0\mathscr{C}gh^3(\alpha_1+\alpha_2)/2\mu D$ |
| $S_{i,j}$ | mean rate of strain $\frac{1}{2}(\frac{\partial U_i}{\partial x_j}+\frac{\partial U_j}{\partial x_i})$ (s$^{-1}$) |
| $Sh$ | Sherwood number $hk_m/D$ |
| $T$ | absolute temperature (K) |
| $\Delta T$ | characteristic temperature difference $T_h - T_c$ (K) |
| $T_c$ | temperature of cold wall (K) |
| $T_h$ | temperature of hot wall (K) |
| $u_x = u_1 = u$ | horizontal velocity (m s$^{-1}$) |
| $u_y = u_2 = v$ | vertical velocity (m s$^{-1}$) |
| $V_+$ | electric potential of the anode, minus the equilibrium electric potential of the cell (V) |

| | |
|---|---|
| $V_-$ | electric potential of the cathode, minus the equilibrium electric potential of the cell (V) |
| $z$ | charge number of species (nondimensional) |
| $z_1 = -z_2 = 2$ | number of electrons involved in electrode reaction |

*Greek symbols*

| | |
|---|---|
| $\alpha_1, \alpha_2$ | volume expansion factors for the metallic and the nonmetallic species respectively |
| $\beta$ | volume expansion factor $(\alpha_1 + \alpha_2)/2$ ($m^3$ $mol^{-1}$) |
| $\delta_{ij}$ | Kronecker delta |
| $\epsilon$ | rate of turbulent kinetic energy dissipation |
| $\eta$ | overpotential $E - E_{eq}$ (V) |
| $\mu$ | dynamic viscosity of solution (kg $m^{-1}$ $s^{-1}$) |
| $v$ | kinematic viscosity $\mu/\rho$ ($m^2$ $s^{-1}$) |
| $\rho$ | fluid density (kg $m^{-3}$) |
| $\phi$ | electric potential (V) |
| $\sigma_\epsilon$ | turbulent Prandtl number for $\epsilon$ set to 1.2174 |
| $\sigma_k$ | turbulent Prandtl number for $k = 1$. |
| $\sigma_T$ | turbulent Prandtl number for temperature 0.9 |

*Subscripts*

| | |
|---|---|
| $\tilde{g}$ | instantaneous value of $(\cdots)$ |
| g | The average value of $(\cdots)$ on time |
| $g' = \tilde{g} - g$ | The fluctuation with time of $(\cdots)$ |
| $(\cdots)^A$ | a value referred to the anode |
| $(\cdots)^C$ | a value referred to the cathode |
| $(\cdots)_1$ | a value referred to the metallic ionic species |
| $(\cdots)_2$ | a value referred to the non metallic ionic species |
| $(\cdots)_{eff}$ | sum of the laminar and the turbulent $(\cdots)$ |
| $(\cdots)_M$ | value $(\cdots)$ in the metallic phase |
| $(\cdots)_{max}$ | maximal value of $(\cdots)$ |
| $(\cdots)_0$ | reference value of $(\cdots)$ |
| $(\cdots)_S$ | value $(\cdots)$ in the liquid phase |
| $(\cdots)_{wall}$ | value of $(\cdots)$ at the wall |
| $(\cdots)_\infty$ | value of $(\cdots)$ far away from the wall |

## 1. Introduction

Electrochemical cells appear in several industrial applications, such as copper refining cells and lead–acid batteries. It turns out that between the different transport mechanisms, convection, migration and diffusion, convection controls in most applications. The fact that the liquid moves due to buoyancy influences the process considerably. The efficiency of the transport mechanisms in turn directly influences the process of interest in the cell. Therefore, during the past few years, hydrodynamics of electrochemical cells have been subject to many scientific and industrial investigations.

Eklund *et al.* [1] studied the flow in a copper refining cell both numerically and experimentally. The concentration field was measured by holographic laser interferometry and the velocity profiles using laser–Doppler velocimetry. The theoretical model was based on hydrodynamic conservation laws. Electrodes kinetics were modelled with a constant concentration flux for copper ions at the electrodes. Very good agreement between theoretical predictions and experimental measurements was found.

In a theoretical investigation, Bark and Alavyoon [2] considered free convection in an electrochemical system with nonlinear reaction kinetics and a binary electrolyte. Unsteady electrolysis was investigated for large values of Rayleigh and Schmidt numbers. The change transfer at the electrodes was mathematically quantified by a Butler–Volmer law. Using perturbation theory, the authors derived a simplified model for the evolution of the system. They found good agreement with results form numerical solutions of the full problem.

Computation of turbulent flow set up by inhomogeneities in the density field, in a closed cavity, is not free from difficulties. The case of flow in a differentially heated square cavity has recently been used as a test for turbulence models and numerical procedures. Henkes and Hoogendoorn [3] reported results of computation of turbulent natural convection in enclosures. The comparison, between different models and solution schemes, aimed at diminishing numerical inaccuracies and at obtaining a numerical reference solution for the differentially heated squared enclosures. To investigate numerical accuracy, a well-defined configuration was prescribed, and the standard $k$–$\epsilon$ model was used as the reference model. Although results close to experimental data were presented, distinct inconsistencies were observed. Computational difficulties such as slow convergence were noted.

In the present work, attention has been paid to flows where turbulent transport has to be taken into account. The commercially available code, CFX F3D, is used for a more detailed investigation of the case studied by Ziegler and Evans [4]. Their work is extended by more accurate simulations and models. Also, a more sophisticated, nonlinear Butler–Volmer law as the boundary condition at the electrodes, is used for the description of the electrodes kinetics. Detailed comparisons are made between predicted results and the literature, for two flow cases.

## 2. Problem formulation

Two electrodes made from same metal are immersed in a dilute solution of a salt of the electrode metal providing a binary electrolyte in a rectangular cell. The two-dimensional cell, which is assumed to have

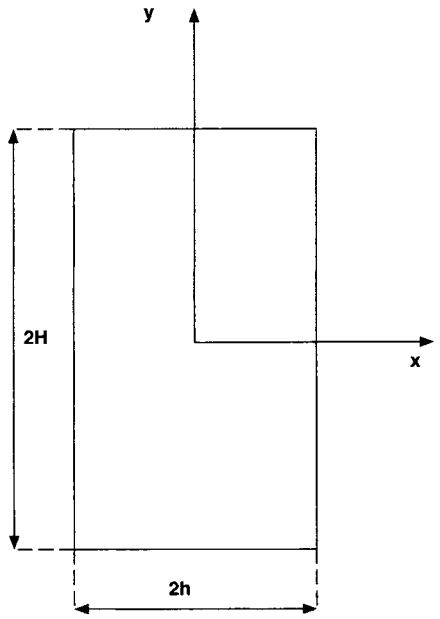


Fig. 1. Geometry of cell and chosen coordinate system.

its sides parallel to the direction of gravity, is shown in Fig. 1. The dissolution of metallic ions generally increases the density of the fluid near the anode. Near the cathode, the reverse reaction takes place resulting in a lower density. Inhomogeneities in the density field set the fluid in motion with a convection pattern downwards near the anode and upwards near the cathode. Convection contributes to transport of ions and thereby influences the chemistry of the cell.

The mathematical model considered by Bark and Alavyoon [2] is reviewed and extended to investigate the case of turbulent flows. The standard turbulence $k$–$\epsilon$ model is used. The present study performed also numerical predictions for the case of Ziegler *et al.* [4] with the low-Reynolds number model. The results are not shown here. As reported by Jones and Launder [5], the low-Reynolds version was found to produce a numerically unstable solution for natural convection in a two-dimensional channel. The hydrodynamic problem must be solved for six dependent variables in a two-dimensional configuration: the concentration fields, $c_1$ and $c_2$, where the subscript 1 denoted the anion, and subscript 2, the corresponding cation, the velocity field $\vec{u} = (u, v, 0)$, the pressure field $p$ and the electric potential $\phi$. Apart from the double layers, the electrolyte can be assumed to be electrically neutral, that is $z_1c_1 + z_2c_2 = 0$, where $z$ denotes the charge number of the species and the indices 1 and 2, the metallic and the nonmetallic ionic species respectively. If the double layer is not to be explicitly accounted for, the mathematical problem can be formulated using a single variable for the concentration fields by defining $c = z_1c_1 = -z_2c_2$, which satisfies the neutrality condition. The governing equations for the above five independent variables assume however, for simulation of turbulent flows, additional terms and equations to take into account the effects of random temporal and spatial fluctuations. Introducing $f$ as time-average value of any variable, and $f'$ its fluctuating part, and introducing the turbulent kinetic energy $k = \frac{1}{2}\overline{u_i'^2}$ ($\mathrm{m^2\,s^{-2}}$), and a rate of turbulent kinetic energy dissipation $\epsilon$ ($\mathrm{m^2\,s^{-3}}$), the following system of equations is obtained for $z_1 = -z_2 = 2$

$$\frac{\partial \vec{u}}{\partial t} + Ra_h \vec{u}\cdot\nabla\vec{u} = Sc\left(-\nabla p + \nabla^2\vec{u} - c\vec{e}_y\right) + \frac{1}{D}\nabla\cdot\left(\nu_T\left(\nabla\vec{u} + (\nabla\vec{u})^T\right)\right) \quad (1)$$

$$\nabla\cdot\vec{u} = 0 \quad (2)$$

$$\frac{\partial c}{\partial t} + Ra_h\vec{u}\cdot\nabla c = \nabla^2 c + \frac{1}{\sigma_T D}\nabla\cdot(\nu_T\nabla c) \quad (3)$$

$$\Gamma\nabla\cdot(1+c)\nabla\phi + \nabla^2 c = 0 \quad (4)$$

$$\rho\frac{\partial k}{\partial t} + \rho\nabla\cdot(k\vec{u}) - \nabla\cdot\left(\left(\mu + \frac{\mu_T}{\sigma_k}\right)\nabla k\right) = P + G - \rho\epsilon \quad (5)$$

$$\rho\frac{\partial \epsilon}{\partial t} + \rho\nabla\cdot(\epsilon\vec{u}) - \nabla\cdot\left(\left(\mu + \frac{\mu_T}{\sigma_\epsilon}\right)\nabla\epsilon\right) = C_1\frac{\epsilon}{k}P - C_2\rho\frac{\epsilon^2}{k} \quad (6)$$

where

$$\mu_T = C_\mu\rho\frac{k^2}{\epsilon}$$

$$\mu_{\mathrm{eff}} = \mu + \mu_T$$

$$P = \mu_{\mathrm{eff}}\nabla\vec{u}\cdot\left(\vec{u} + (\vec{u})^T\right)$$

$$G = \frac{-\mu_{\mathrm{eff}}}{\rho\cdot\sigma_T}\vec{g}\cdot\nabla\rho$$

$Ra_h$, $Sc$, $D$ and $\Gamma$ are defined as

$$Ra_h = \frac{\rho_0\mathscr{C}gh^3(\alpha_1+\alpha_2)}{2\mu D}, \quad Sc = \frac{\mu}{\rho_0 D} \quad (7)$$

$$D = \frac{2D_1D_2}{D_1+D_2}, \quad \Gamma = \frac{2(D_1+D_2)}{D_1-D_2} \quad (8)$$

$\mathscr{C}$ is defined as min $[\frac{hi_0}{FD_1}\times\sinh[\frac{F}{RT}(V_+ - V_+)], c_0]$ [2], or min $[\frac{hi}{2FD_1}, c_0]$ when $\partial C/\partial n$ is set constant at the electrodes [4]. The above system is set for the non-dimensional variables $\vec{x}^*$, $\vec{v}^*$, $t^*$, $\phi^*$, $\vec{i}^*$ and $c^*$, where $^*$ superscripts are dropped. The nondimensional variables can be defined as

$$\vec{x} = \vec{x}^* h, \quad \vec{v} = \frac{\rho_0\mathscr{C}gh^2(\alpha_1+\alpha_2)}{2\mu}\vec{v}^*, \quad t = \frac{h^2}{D}t^* \quad (9)$$

$$\phi + \frac{V_+ + V_-}{2} = \frac{RT}{F}\phi^*, \quad \vec{i} = i_0\vec{i}^*, \quad c^* = \frac{c-c_0}{\mathscr{C}} \quad (10)$$

A series of numerical calculations, calculated for the turbulent case of Ziegler *et al.* [4], proved that $G$ does not influence the prediction of the mean velocity, and can be neglected in the transport equation for $k$.

Ozoe [6] performed a sensitivity analysis for the constants of the $k$–$\epsilon$ turbulent model and determined different values for $C_1$ and $\sigma_T$ rather than those listed below. However, since the applicability of these values for different geometric and boundary conditions

is not known, they were not employed here. The turbulent constants are therefore chosen as Henkes [3], except for $C_\epsilon$ in the buoyant term of the $\epsilon$ equati on, which was shown to have no significant influence on the solutions: $C_1 = 1.44$, $C_2 = 1.92$, $C_\epsilon = 0$, $C_\mu = 0.09$, $\sigma_T = 0.9$, $\sigma_k = 1$ and $\sigma_\epsilon = 1.3$.

A turbulent contribution should also be taken into account for the calculation of the electrical potential. Here, it is assumed that the turbulent contribution is negligible.

Bark and Alavyoon [1] used a semiempirical Butler–Volmer law and formulated the following non-dimensional boundary conditions at the anode and cathode

$$\frac{\partial c}{\partial x} = \begin{cases} \frac{hi_0}{2FD_1\mathscr{C}}\left[e^{(\upsilon-\phi)} - (1+c)e^{(\phi-\upsilon)}\right] \\ \quad \text{at } x = -1,\ |y| \le \mathscr{H} \text{ (anode)} \\ -\frac{hi_0}{2FD_1\mathscr{C}}\left[(1+c)e^{(\phi+\upsilon)} - e^{-(\phi+\upsilon)}\right] \\ \quad \text{at } x = +1,\ |y| \le \mathscr{H} \text{ (cathode)} \end{cases} \tag{11}$$

where $\mathscr{V} = \frac{F}{2RT}(V_+ - V_-)$, and $\mathscr{H} = H/h$. Here the formula was not modified to account for turbulent fluctuations. Ziegler and Evans [4], used a simpler condition

$$\frac{\partial c}{\partial x} = \text{constant} \tag{12}$$

For the electrical potential, because $\vec{N}_2 \cdot \vec{e}_x = \vec{0}$ at $x = \pm 1$,

$$(1+c)\frac{\partial \phi}{\partial x} = \frac{1}{2}\frac{\partial c}{\partial x} \quad \text{at } x = \pm 1,\ |y| \le \mathscr{H} \text{ (anode, cathode)} \tag{13}$$

No transfer of mass occurs at the horizontal walls, resulting in vanishing normal derivatives of the concentration and potential fields

$$\frac{\partial c}{\partial y} = \frac{\partial \phi}{\partial y} = 0 \quad \text{at } y = \pm\mathscr{H},\ |x| \le 1 \tag{14}$$

For the velocity field, no slip conditions are applied on all four walls, that is

$$\vec{u} = \vec{0} \quad \text{at } x = \pm 1 \text{ and } y = \pm\mathscr{H} \tag{15}$$

## 3. Methodology

The set of equations is solved numerically using the commercial code CFX F3D [7]. The solution methodology is based on the finite volume discretization of the transport equations and the continuity equation for all incompressible fluid. The numerical scheme is based on the pressure correction method. The pressure-correction equation is obtained by applying the SIMPLE algorithm [8] to the momentum equations. The Rhie and Chow [9] interpolation scheme is used to prevent chequerboard oscillations of pressure on the colocated grid. In the present computations, full field Stone's method was used to solve the velocity variables, concentration and the preconditioned conjugate gradients for pressure. The advection term was discretized using an upwind method for steady computation. During simulation of unsteady flow, in addition to the finer mesh, CCCT [10], which is a more stable formulation of the QUICK scheme, was used. The use of CCCT decreases numerical diffusions and makes a study of small fluctuations possible.

## 4. Results

In this Section, results from numerical investigations of the two-dimensional flow in an electrochemical cell are presented. The Rayleigh and Grashof number are based on the half-width of the cell. The same parameters used by Ziegler and Evans [4], are first chosen so that the results can be compared with their theoretical and experimental investigations. The flow is then studied in more detail.

The flow is assumed to take place in a cell with a width of 2.4 cm and a height of 85 cm. The Rayleigh number is $5 \times 10^9$ and the Schmidt number 2763. The vertical walls of the cell form the anode and cathode, where mass flux is set constant. The horizontal walls are electrically isolated. A detailed set of the parameters involved in the simulation is given in Table 1.

The simulation was started with a mesh similar to that used by Ziegler and Evans, $32 \times 22$ mesh points in the vertical and horizontal directions, respectively. As in that work, the equations were solved assuming a steady state and the standard form of the $k$–$\epsilon$ turbulence model. Figure 2 shows the mean vertical velocity at the mid-height of the cell. The predicted velocity profile agrees qualitatively well with the experimental data.

The same calculation was repeated with a finer mesh using $200 \times 50$ mesh points in the vertical and horizontal directions, respectively. In order to study the possible oscillations, after the initial transients are dampened out, the flow was first simulated under assumption of steady-state. Thereafter, the simulation was continued as time dependent flow. Figure 3 shows a comparison between the predicted vertical velocity profile, as a function of time, and the measurements of Ziegler and Evans. The agreement with experimental data, compared to that of Fig. 2, is clearly improved. The thickness of the boundary layer on the wall is nicely predicted.

*Table 1. Physical parameters of flow studied by Ziegler and Evans [4]*

| *Quantity* | *Value* |
|---|---|
| Ionic metal | Cadmium, $Cd^{++}$ |
| Average salt diffusivity | $5.76 \times 10^{-10}$ m$^2$ s$^{-1}$ |
| Average viscosity | $1.91 \times 10^{-3}$ kg (m s)$^{-1}$ |
| Average density | 1200 kg m$^{-3}$ |
| Relative variation in density with solute fraction | 1.97 |
| Reference concentration | 0.0937 (mass fraction) |
| Anode-cathode spacing | 0.024 m |
| Cell height | 0.85 m |
| Current density | 100 A m$^{-2}$ |

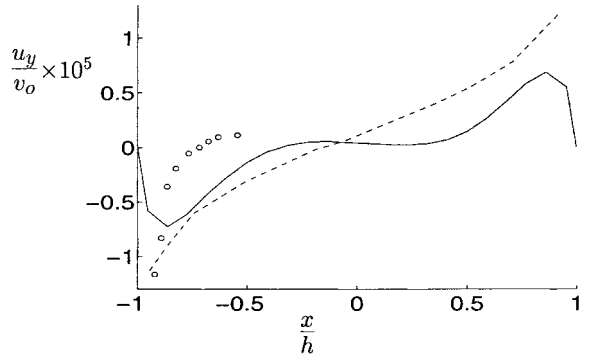


Fig. 2. Vertical mean velocity at midheight of the cell. Result from present computation (solid line) is composed with theoretical (dashed line) and experimental data (dots) obtained by Ziegler and Evans. $Ra_h = 5 \times 10^9$, $Sc = 2763$.

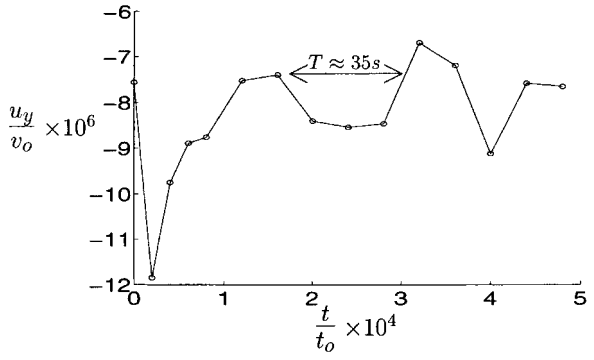


Fig. 4. Maximal vertical mean velocity in boundary layer near anode, in an horizontal cross section of the cell at its midheight, as a function of time. $Ra_h = 5 \times 10^9$, $Sc = 2763$.

Figure 4 shows the present simulation of the maximum velocity inside the boundary layer at the mid-height of the cell as a function of time. After about 20 s, regular fluctuations with a period of about 35 s, is observed. The magnitude of the fluctuations is less than 10% of the mean value.

The maximum mean velocity at the mid-height of the cell is $-6.75 \times 10^{-4}\,\mathrm{m\,s^{-1}}$. By comparing this vertical velocity, with the period of fluctuations and the width of the cell, fluctuations in the velocity field can be attributed to advection of wave-like eddies whose size is of the same order of magnitude as the width of the cell. Figure 5 shows that a wavy structure can be found in the boundary layer, with a wavelength comparable to the width of the cell. The waves travel at a speed close to that of the maximum velocity in the wall-layer.

For the same geometry, with two heated vertical walls, a Prandtl number of 7 and Rayleigh numbers based on the half-width of the cell around $7.234 \times 10^5$, Elder [11] observed a similar wavy boundary layer structure and similar trend in the wavelength. Elder stated that the wall waves appeared when the flow was close to transition to turbulence and could be seen as instabilities in the boundary layer. The wave train lost its regularity as the turbulent state was approached.

At higher current densities, the flow becomes, loosely speaking, more like conventional turbulence, where small scale turbulent fluctuations become dominant, in comparison with large structures of sizes comparable to the width of the cell. Figure 6 shows the increase in mean velocity with current density. The calculations were run using a coarse grid, which, as previously shown, predicted the flows qualitatively well.

It was found empirically on the basis of the computational effort of the present study, that the maximal mean velocity is approximately given by the relation

$$v_{\max} = \lambda \times i^{0.51} \tag{16}$$

where $v_{\max}$ and $i$ are given in $\mathrm{m\,s^{-1}}$ and $\mathrm{A\,m^{-2}}$, respectively, and $\lambda = 1.23 \times 10^{-4}\,\mathrm{m^{2.02}\,s^{-1}\,A^{-0.51}}$. This relation is in relative agreement with the one found out by Ziegler and Evans, who found $\lambda = 2.33 \times 10^{-4}\,\mathrm{m^{2.02}\,s^{-1}\,A^{-0.51}}$. In accordance with Ziegler and Evans, a constant current density was imposed at electrodes. An alternative way, of modelling the charge transfer at the electrodes, is use a Butler– Volmer law. It allows a study of the influence of current density distribution on flow. However, as discussed by Bark and Alavyoon [2], the use of it, due to numerical complexities, limits the computations to

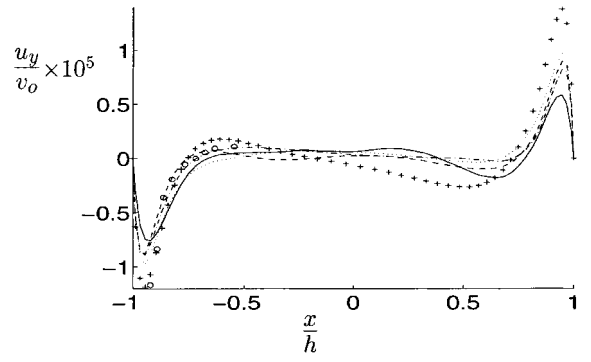


Fig. 3. Vertical mean velocity at midheight of the cell, at different moments of time, for the first 20 s, at each 5 s. Dots represent the experimental data by Ziegler and Evans. $Ra_h = 5 \times 10^9$, $Sc = 2763$.

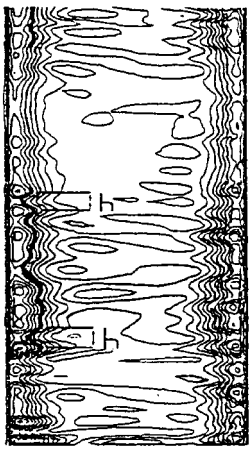


Fig. 5. Isolines of vertical velocity. Horizontal dimension is expanded by a factor 10. Distances equal to the width of the cell are marked at two different vertical positions. $Ra_h = 5 \times 10^9$, $Sc = 2763$.

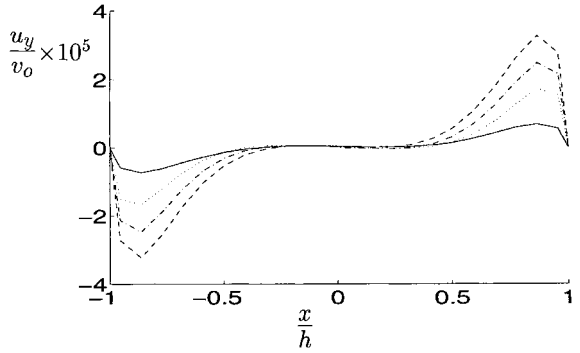


Fig. 6. Influence of the current density ($I$) on the velocity field for constant values of current density on the electrodes. $Sc = 2763$. ($I/\mathrm{A\,m^{-2}}$, $Ra_\mathrm{h}$): (—) 100, $5\times10^9$; (· · · · ·) 200, $1\times10^{10}$; (-·-·-·) 300, $1.5\times10^{10}$; (- - - -) 400, $2\times10^{10}$.

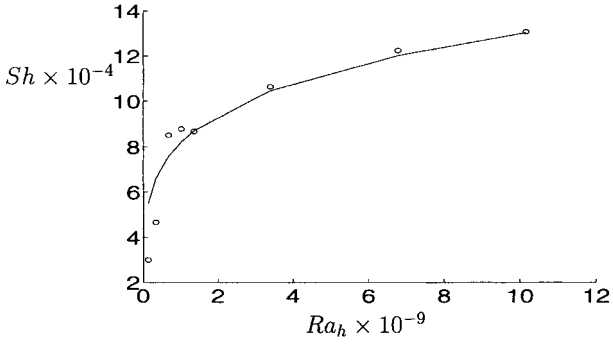


Fig. 8. Variation of Sherwood number for different Rayleigh numbers. Diamonds show the predicted Sherwood numbers, while the solid line presents empirical correlation curve, $Sh = Ra_\mathrm{h}^{0.2}$.

very low cell potential drops. Figure 7 shows the current density distribution along the cathode for two different exchange current densities. The computed current densities are normalized by dividing by their maximum value, which, according to Fig. 7, was found, as expected, at the bottom of the cell. The exchange current density was varied by a factor of 10, between the two cases, resulting in a maximal computed current density of about three times larger for the highest value. The current density varied linearly in the vertical direction apart from the close neighbourhood to the vertical boundaries. The imposed potential difference between anode and cathode was 0.014 V in the above simulation.

The Sherwood number is the nondimensional mass flux at the electrodes, and is defined as $\frac{H}{C_\mathrm{wall}-C_\infty}\left[\frac{\partial C}{\partial n}\right]_\mathrm{wall}$ [12]. Here attention is paid to the qualitative dependence of the Sherwood number on the Rayleigh number, and therefore, the details in the scaling procedure are of minor importance. Figure 8 shows the computed Sherwood number. This number is calculated at the cathode, at the midheight of the cell which, due to the almost linear variation of the current density, equals the mean Sherwood number. The numerical predicted Sherwood number is found to be related to the Rayleigh number according to $Sh \approx Ra_\mathrm{h}^{0.2}$. The Rayleigh number, in the above formula, is based on the width of the cell. The reader is referred to Elder [11] for details on the choice of the relevant scales.

Henkes and Hoogerdoorn [3] observed that the wall functions, used in the standard $k$–$\epsilon$ model formulation, have been established for forced convection. This means that they are not adapted for natural convection and thus he proposed to impose a fixed and large value for $\epsilon$ at the first mesh points. An imposed value for $\epsilon$, corresponds to a nondimensional distance $y^+_\mathrm{wall} = C_\mu/(0.41\,v\,k^2\epsilon)$ from the wall to the first mesh point. Henkes showed (see Appendix A) that setting a high value of $\epsilon$ gave good results and that the computed variables were found to be independent of the value, as soon as it is large enough. In other words, the results are not very sensitive to the nondimensional distance between the first mesh point and the wall. Unfortunately, this is not the case for flows where the flux is given for the walls, for example in electrochemical systems. Figure 9 shows the sensitivity of the flow, to the imposed value $y^+_\mathrm{wall}$ at the first mesh points. Fortunately, as shown above, the traditional wall functions predict results in good agreement with the experimental data.

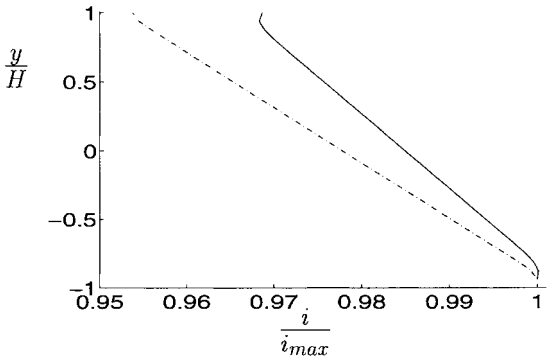


Fig. 7. Predicted current density distribution using the Butler–Volmer law at two different exchange current densities. Current density is normalized by the maximal predicted value. Solid line corresponds to the lower value of the exchange current density, $1\,\mathrm{A\,m^{-2}}$ and dashed line to the case 10 times higher.

## 5. Conclusions

The study of the turbulent case considered by Ziegler and Evans [4] revealed the presence of large scale turbulent fluctuations, estimated close to the width of

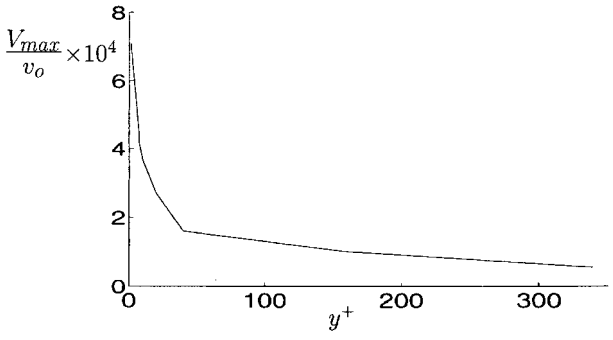


Fig. 9. $V_\mathrm{max}$ against $y^+$. $Ra_\mathrm{h} = 5\times10^9$, $Sc = 2763$.

the cell, and indicating local sites of weak turbulence near the transitional state. The standard $k$–$\epsilon$ model was used for the prediction of a transitional flow induced by natural convection, and good agreement was also obtained with previous direct simulations [13]. Results are shown in Appendix B. The nonlinear kinetics were simulated using a formula derived from a Butler-Volmer law. The predicted Sherwood number was found to be approximately proportional to the Rayleigh number to the power 0.2.

## 6. Appendices: Validation of the code

### 6.1. *Appendix A: Turbulent free convection in a closed cavity*

Turbulent free convection in a closed cavity has been a test case for turbulence models and numerical methods, see [3]. The flow to be computed takes place in a square cavity and can be assumed to be two-dimensional. The cavity contains air, resulting in a Prandtl number of 0.7. The flow is driven by a temperature difference between vertical walls, while the horizontal walls are assumed to be isolated. The Rayleigh number, based on the temperature difference and the width, or height, of the cavity, is set to $Ra = 5 \times 10^{10}$. The turbulence model used here is the standard $k$–$\epsilon$ model without any modifications. As recommended by Henkes and Hoogerdoorn [3], the value of $\epsilon$ in the first cell near the vertical wall was set to a large value. The simulations was run using $90 \times 90$ mesh points, with a higher concentration of grid points near the wall, than in the centre of the cavity.

In Figs 10 and 11, the nondimensional vertical velocity and the turbulent kinetic energy, along a horizontal cross section at the midheight of the cell, are presented. In those Figures, results from the present study are compared with those from numerical simulations reported by Henkes *et al.* and experimental data. The temperature variation, on a vertical cross section in the midplane of the cell, is presented in Fig. 12.

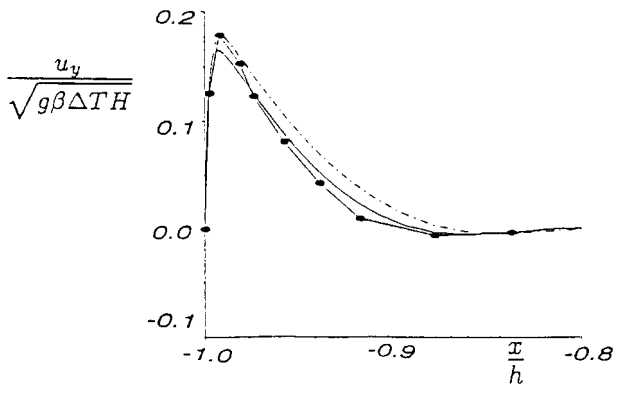


Fig. 10. Mean nondimensional vertical velocity profile at the midheight of the cell. Key: (—) Henkes *et al.*; (·····) present study; (•) Cheesewright *et al.* (1986) [14] (experimental).

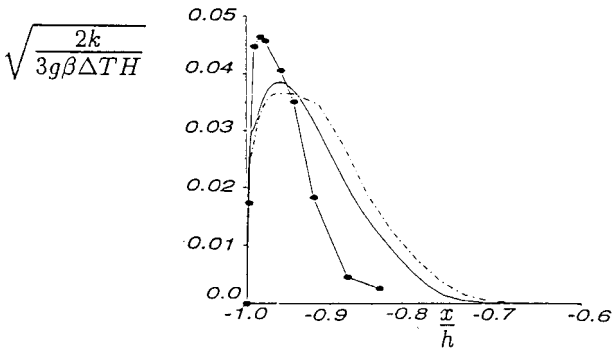


Fig. 11. Mean turbulent kinetic energy near the wall, on a cross section at $y = 0$. $Ra = 5 \times 10^{10}$, $Pr = 0.71$. Key: (—) Henkes *et al.*; (·····) present study; (•) Cheesewright *et al.* (1986) [14] (experimental).

Figure 13 shows a comparison between the computed nondimensional heat flux, the Nusselt number, along the hot wall from the present simulation. It also shows the same prediction by Henkes *et al.* and experimental data. Figure 14 presents a similar comparison, for the nondimensional shear stress along the hot wall. Fluxes at the wall are quantities, related to gradient of the field variables, and therefore less accuracy can be expected in their prediction. Similar deviations from experimental

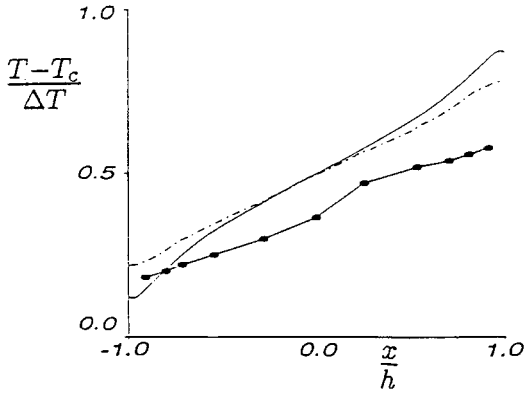


Fig. 12. Nondimensional temperature profile in the medium vertical cross section of the cell. $Ra = 5 \times 10^{10}$, $Pr = 0.71$. Key: (—) Henkes *et al.*; (·····) present study; (•) Cheesewright and Ziai (1986) [15] (experimental).

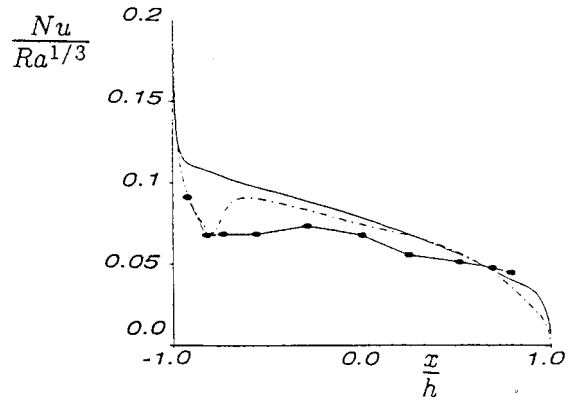


Fig. 13. Nondimensional wall heat transfer along the hot wall. $Ra = 5 \times 10^{10}$, $Pr = 0.71$. Key: (—) present study; (·····) Henkes *et al.*; (•) King (1989) [16] (experimental).

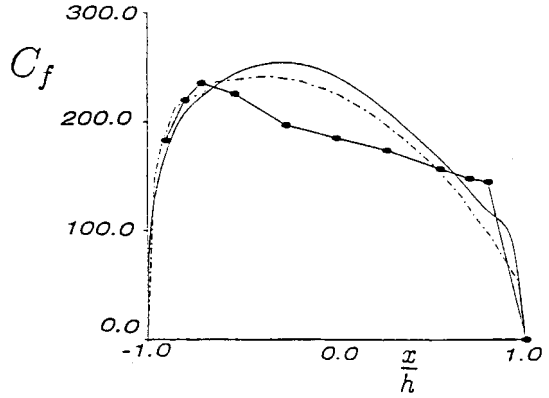


Fig. 14. Nondimensional wall shear stress along the hot wall. $Ra = 5 \times 10^{10}$, $Pr = 0.71$. Key: (—) present study; (·····) Henkes *et al.*; (•) King (1989) [16] (experimental).

data have been observed in earlier numerical predictions, see [3].

The boundary conditions for the $\epsilon$ equation has been discussed in different contributions. The numerical solution found by Henkes *et al.* for the Nusselt at the hot wall, as shown in Fig. 13, reveals a local and abrupt decay of the Nusselt on the lower part of the wall. This decay is identified [3] as the transition point of the boundary layer to the turbulent regime. Such a transition point has not been observed here with the conventional $k$–$\epsilon$ model.

### 6.2. *Appendix B: Turbulent unstratified natural convection in a vertical slot for Pr = 0.71*

The computed flow takes place in an infinite vertical canal, so that it is imposed periodic boundary conditions in the vertical direction. A fixed difference of normalized temperature is set to 1 between the two vertical walls. The Grashof number is set consecutively to 8100 and 22 500, see Figs 15 and 16. The Prandtl number is 0.71. Calculations performed by

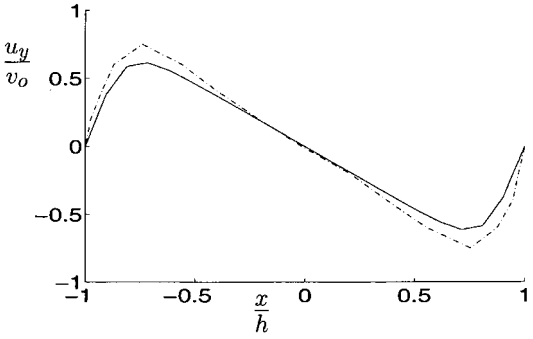


Fig. 15. Nondimensional velocity profile in an horizontal cross section of the cell. $Gr_h = 8100$, $Pr = 0.71$. Key: (—) present study; (·····) Phillips [13].

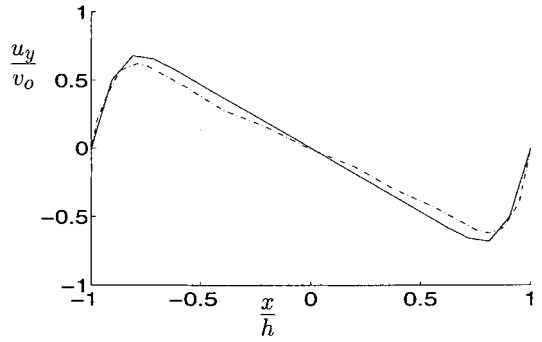


Fig. 16. Nondimensional velocity profile in an horizontal cross section of the cell. $Gr_h = 22\,500$, $Pr = 0.71$. Key: (—) present study; (·····) Phillips [13].

the present study were two-dimensional and used the $k$–$\epsilon$ model in its standard version. The result are compared with the direct simulations performed by Phillips [13].

As Phillips reported, "at a Prandtl number of 0.7, the critical Grashof number is 8041". Figure 15 is then typically a case of transitional flow. The $k$–$\epsilon$ model is nevertheless able to predict the velocity profile qualitatively well. For higher Grashof number, the prediction performed with the $k$–$\epsilon$ model is still valid as the turbulent site is approached, see Fig. 16.

## References

[1] A. Eklund, F. Alavyoon, D. Simonsson, R.I. Karlsson and F.H. Bark, *Electrochim. Acta* **36** (1991) 1345.
[2] F. H. Bark and F. Alavyoon, *J. Fluid Mech.* **290** (1995) 1.
[3] R. A. Henkes and C. J. Hoogendoorn, *Num. Heat Transfer.* **28** (1995) 59.
[4] D. Ziegler and J. W. Evans (1986) *J. Electrochem. Soc.* **133** (1986) 559.
[5] W. P. Jones and B. E. Launder, *Int. J. Heat Mass Transfer* **15** (1972) 301.
[6] H. Ozoe, A. Mouri, M. Ohmuro, S.W. Churchill and N. Lior, *ibid.* **28** (1985) 125.
[7] CFX-F3D release 3.3: 'User Manual', AEA Technology-Computational Fluid Dynamics Services, Building 8.19, Harwell Laboratory, Oxfordshire OX11 0RA, UK, (1994).
[8] S. V. Patankar and D. B. Spalding, *Int. J. Heat Mass Transfer* **15** (1972) 1787.
[9] C. M. Rhie and W. L. Chow, *Am. Institute of Aeronautics and Astronautics J.* **21** (1983) 1527.
[10] P. H. Gaskell and A. K. C Lau, Proceedings of the Conference on 'Numerical Methods in Laminar and Turbulent Flow', Montreal (1987).
[11] J. W. Elder, *J. Fluid Mech.* **23** (1965) 99.
[12] A. Bejan, 'Convection Heat Transfer' 2nd edn. Wiley, (J. & Sons, New York, 1995).
[13] J. R. Phillips, *Int. J. Heat. Mass Transfer* **39** (1996) 2485.
[14] R. Cheesewright, K.J. King and S. Ziai, *Proc. ASME Meeting HTD* **60** (1986) 75.
[15] R. Cheesewright and S. Ziai, Proceedings of the 8th International Heat Transfer Conference, San Francisco (1986) 1465.
[16] K. J. King, Turbulent Natural Convection in Rectangular Air Cavities, Ph.D. Thesis, Queen Mary College, London, UK (1989).